UC Berkeley

UC Berkeley Previously Published Works

Title

Searches for the baryon- and lepton-number violating decays B0→Λc+l-, B-→Λl-, and B-→Λ¯l-

Permalink

https://escholarship.org/uc/item/8fw6983m

Journal

Physical Review D, 83(9)

ISSN

2470-0010

Authors

del Amo Sanchez, P
Lees, JP
Poireau, V
et al.

Publication Date

2011-05-01

DOI

10.1103/physrevd.83.091101

Copyright Information

This work is made available under the terms of a Creative Commons Attribution License, availalbe at https://creativecommons.org/licenses/by/4.0/

Peer reviewed

eScholarship.org Powered by the California Digital Library
University of California

PHYSICAL REVIEW D **83,** 091101(R) (2011)

Searches for the baryon- and lepton-number violating decays $B^0 \to \Lambda_c^+ l^-$, $B^- \to \Lambda l^-$, and $B^- \to \bar{\Lambda} l^-$

P. del Amo Sanchez,[1] J. P. Lees,[1] V. Poireau,[1] E. Prencipe,[1] V. Tisserand,[1] J. Garra Tico,[2] E. Grauges,[2] M. Martinelli,[3a,3b] D. A. Milanes,[3a] A. Palano,[3a,3b] M. Pappagallo,[3a,3b] G. Eigen,[4] B. Stugu,[4] L. Sun,[4] D. N. Brown,[5] L. T. Kerth,[5] Yu. G. Kolomensky,[5] G. Lynch,[5] I. L. Osipenkov,[5] H. Koch,[6] T. Schroeder,[6] D. J. Asgeirsson,[7] C. Hearty,[7] T. S. Mattison,[7] J. A. McKenna,[7] A. Khan,[8] V. E. Blinov,[9] A. R. Buzykaev,[9] V. P. Druzhinin,[9] V. B. Golubev,[9] E. A. Kravchenko,[9] A. P. Onuchin,[9] S. I. Serednyakov,[9] Yu. I. Skovpen,[9] E. P. Solodov,[9] K. Yu. Todyshev,[9] A. N. Yushkov,[9] M. Bondioli,[10] S. Curry,[10] D. Kirkby,[10] A. J. Lankford,[10] M. Mandelkern,[10] E. C. Martin,[10] D. P. Stoker,[10] H. Atmacan,[11] J. W. Gary,[11] F. Liu,[11] O. Long,[11] G. M. Vitug,[11] C. Campagnari,[12] T. M. Hong,[12] D. Kovalskyi,[12] J. D. Richman,[12] C. A. West,[12] A. M. Eisner,[13] C. A. Heusch,[13] J. Kroseberg,[13] W. S. Lockman,[13] A. J. Martinez,[13] T. Schalk,[13] B. A. Schumm,[13] A. Seiden,[13] L. O. Winstrom,[13] C. H. Cheng,[14] D. A. Doll,[14] B. Echenard,[14] D. G. Hitlin,[14] P. Ongmongkolkul,[14] F. C. Porter,[14] A. Y. Rakitin,[14] R. Andreassen,[15] M. S. Dubrovin,[15] B. T. Meadows,[15] M. D. Sokoloff,[15] P. C. Bloom,[16] W. T. Ford,[16] A. Gaz,[16] M. Nagel,[16] U. Nauenberg,[16] J. G. Smith,[16] S. R. Wagner,[16] R. Ayad,[17,*] W. H. Toki,[17] H. Jasper,[18] A. Petzold,[18] B. Spaan,[18] M. J. Kobel,[19] K. R. Schubert,[19] R. Schwierz,[19] D. Bernard,[20] M. Verderi,[20] P. J. Clark,[21] S. Playfer,[21] J. E. Watson,[21] M. Andreotti,[22a,22b] D. Bettoni,[22a] C. Bozzi,[22a] R. Calabrese,[22a,22b] A. Cecchi,[22a,22b] G. Cibinetto,[22a,22b] E. Fioravanti,[22a,22b] P. Franchini,[22a,22b] I. Garzia,[22a,22b] E. Luppi,[22a,22b] M. Munerato,[22a,22b] M. Negrini,[22a,22b] A. Petrella,[22a,22b] L. Piemontese,[22a] R. Baldini-Ferroli,[23] A. Calcaterra,[23] R. de Sangro,[23] G. Finocchiaro,[23] M. Nicolaci,[23] S. Pacetti,[23] P. Patteri,[23] I. M. Peruzzi,[23,†] M. Piccolo,[23] M. Rama,[23] A. Zallo,[23] R. Contri,[24a,24b] E. Guido,[24a,24b] M. Lo Vetere,[24a,24b] M. R. Monge,[24a,24b] S. Passaggio,[24a] C. Patrignani,[24a,24b] E. Robutti,[24a] B. Bhuyan,[25] V. Prasad,[25] C. L. Lee,[26] M. Morii,[26] A. J. Edwards,[27] A. Adametz,[28] J. Marks,[28] U. Uwer,[28] F. U. Bernlochner,[29] M. Ebert,[29] H. M. Lacker,[29] T. Lueck,[29] A. Volk,[29] P. D. Dauncey,[30] M. Tibbetts,[30] P. K. Behera,[31] U. Mallik,[31] C. Chen,[32] J. Cochran,[32] H. B. Crawley,[32] W. T. Meyer,[32] S. Prell,[32] E. I. Rosenberg,[32] A. E. Rubin,[32] A. V. Gritsan,[33] Z. J. Guo,[33] N. Arnaud,[34] M. Davier,[34] D. Derkach,[34] J. Firmino da Costa,[34] G. Grosdidier,[34] F. Le Diberder,[34] A. M. Lutz,[34] B. Malaescu,[34] A. Perez,[34] P. Roudeau,[34] M. H. Schune,[34] J. Serrano,[34] V. Sordini,[34,‡] A. Stocchi,[34] L. Wang,[34] G. Wormser,[34] D. J. Lange,[35] D. M. Wright,[35] I. Bingham,[36] C. A. Chavez,[36] J. P. Coleman,[36] J. R. Fry,[36] E. Gabathuler,[36] D. E. Hutchcroft,[36] D. J. Payne,[36] C. Touramanis,[36] A. J. Bevan,[37] F. Di Lodovico,[37] R. Sacco,[37] M. Sigamani,[37] G. Cowan,[38] S. Paramesvaran,[38] A. C. Wren,[38] D. N. Brown,[39] C. L. Davis,[39] A. G. Denig,[40] M. Fritsch,[40] W. Gradl,[40] A. Hafner,[40] K. E. Alwyn,[41] D. Bailey,[41] R. J. Barlow,[41] G. Jackson,[41] G. D. Lafferty,[41] J. Anderson,[42] R. Cenci,[42] A. Jawahery,[42] D. A. Roberts,[42] G. Simi,[42] J. M. Tuggle,[42] C. Dallapiccola,[43] E. Salvati,[43] R. Cowan,[44] D. Dujmic,[44] G. Sciolla,[44] M. Zhao,[44] D. Lindemann,[45] P. M. Patel,[45] S. H. Robertson,[45] M. Schram,[45] P. Biassoni,[46a,46b] A. Lazzaro,[46a,46b] V. Lombardo,[46a] F. Palombo,[46a,46b] S. Stracka,[46a,46b] L. Cremaldi,[47] R. Godang,[47,§] R. Kroeger,[47] P. Sonnek,[47] D. J. Summers,[47] X. Nguyen,[48] M. Simard,[48] P. Taras,[48] G. De Nardo,[49a,49b] D. Monorchio,[49a,49b] G. Onorato,[49a,49b] C. Sciacca,[49a,49b] G. Raven,[50] H. L. Snoek,[50] C. P. Jessop,[51] K. J. Knoepfel,[51] J. M. LoSecco,[51] W. F. Wang,[51] L. A. Corwin,[52] K. Honscheid,[52] R. Kass,[52] N. L. Blount,[53] J. Brau,[53] R. Frey,[53] O. Igonkina,[53] J. A. Kolb,[53] R. Rahmat,[53] N. B. Sinev,[53] D. Strom,[53] J. Strube,[53] E. Torrence,[53] G. Castelli,[54a,54b] E. Feltresi,[54a,54b] N. Gagliardi,[54a,54b] M. Margoni,[54a,54b] M. Morandin,[54a] M. Posocco,[54a] M. Rotondo,[54a] F. Simonetto,[54a,54b] R. Stroili,[54a,54b] E. Ben-Haim,[55] M. Bomben,[55] G. R. Bonneaud,[55] H. Briand,[55] G. Calderini,[55] J. Chauveau,[55] O. Hamon,[55] Ph. Leruste,[55] G. Marchiori,[55] J. Ocariz,[55] J. Prendki,[55] S. Sitt,[55] M. Biasini,[56a,56b] E. Manoni,[56a,56b] A. Rossi,[56a,56b] C. Angelini,[57a,57b] G. Batignani,[57a,57b] S. Bettarini,[57a,57b] M. Carpinelli,[57a,57b,‖] G. Casarosa,[57a,57b] A. Cervelli,[57a,57b] F. Forti,[57a,57b] M. A. Giorgi,[57a,57b] A. Lusiani,[57a,57c] N. Neri,[57a,57b] E. Paoloni,[57a,57b] G. Rizzo,[57a,57b] J. J. Walsh,[57a] D. Lopes Pegna,[58] C. Lu,[58] J. Olsen,[58] A. J. S. Smith,[58] A. V. Telnov,[58] F. Anulli,[59a] E. Baracchini,[59a,59b] G. Cavoto,[59a] R. Faccini,[59a,59b] F. Ferrarotto,[59a] F. Ferroni,[59a,59b] M. Gaspero,[59a,59b] L. Li Gioi,[59a] M. A. Mazzoni,[59a] G. Piredda,[59a] F. Renga,[59a,59b] C. Buenger,[60] T. Hartmann,[60] T. Leddig,[60] H. Schröder,[60] R. Waldi,[60] T. Adye,[61] E. O. Olaiya,[61] F. F. Wilson,[61] S. Emery,[62] G. Hamel de Monchenault,[62] G. Vasseur,[62] Ch. Yèche,[62] M. T. Allen,[63] D. Aston,[63] D. J. Bard,[63] R. Bartoldus,[63] J. F. Benitez,[63] C. Cartaro,[63] M. R. Convery,[63] J. Dorfan,[63] G. P. Dubois-Felsmann,[63] W. Dunwoodie,[63] R. C. Field,[63] M. Franco Sevilla,[63] B. G. Fulsom,[63] A. M. Gabareen,[63] M. T. Graham,[63] P. Grenier,[63] C. Hast,[63] W. R. Innes,[63] M. H. Kelsey,[63] H. Kim,[63] P. Kim,[63] M. L. Kocian,[63] D. W. G. S. Leith,[63] P. Lewis,[63] S. Li,[63] B. Lindquist,[63] S. Luitz,[63] V. Luth,[63] H. L. Lynch,[63] D. B. MacFarlane,[63] D. R. Muller,[63] H. Neal,[63] S. Nelson,[63] C. P. O'Grady,[63] I. Ofte,[63] M. Perl,[63] T. Pulliam,[63] B. N. Ratcliff,[63] A. Roodman,[63] A. A. Salnikov,[63] V. Santoro,[63] R. H. Schindler,[63] J. Schwiening,[63] A. Snyder,[63] D. Su,[63] M. K. Sullivan,[63] S. Sun,[63]

 © 2011 American Physical Society

K. Suzuki,[63] J. M. Thompson,[63] J. Va'vra,[63] A. P. Wagner,[63] M. Weaver,[63] W. J. Wisniewski,[63] M. Wittgen,[63] D. H. Wright,[63] H. W. Wulsin,[63] A. K. Yarritu,[63] C. C. Young,[63] V. Ziegler,[63] X. R. Chen,[64] W. Park,[64] M. V. Purohit,[64] R. M. White,[64] J. R. Wilson,[64] A. Randle-Conde,[65] S. J. Sekula,[65] M. Bellis,[66] P. R. Burchat,[66] T. S. Miyashita,[66] S. Ahmed,[67] M. S. Alam,[67] J. A. Ernst,[67] B. Pan,[67] M. A. Saeed,[67] S. B. Zain,[67] N. Guttman,[68] A. Soffer,[68] P. Lund,[69] S. M. Spanier,[69] R. Eckmann,[70] J. L. Ritchie,[70] A. M. Ruland,[70] C. J. Schilling,[70] R. F. Schwitters,[70] B. C. Wray,[70] J. M. Izen,[71] X. C. Lou,[71] F. Bianchi,[72a,72b] D. Gamba,[72a,72b] M. Pelliccioni,[72a,72b] L. Lanceri,[73a,73b] L. Vitale,[73a,73b] N. Lopez-March,[74] F. Martinez-Vidal,[74] A. Oyanguren,[74] H. Ahmed,[75] J. Albert,[75] Sw. Banerjee,[75] H. H. F. Choi,[75] K. Hamano,[75] G. J. King,[75] R. Kowalewski,[75] M. J. Lewczuk,[75] C. Lindsay,[75] I. M. Nugent,[75] J. M. Roney,[75] R. J. Sobie,[75] T. J. Gershon,[76] P. F. Harrison,[76] T. E. Latham,[76] E. M. T. Puccio,[76] H. R. Band,[77] S. Dasu,[77] K. T. Flood,[77] Y. Pan,[77] R. Prepost,[77] C. O. Vuosalo,[77] and S. L. Wu[77]

(*BABAR* Collaboration)

[1]*Laboratoire d'Annecy-le-Vieux de Physique des Particules (LAPP), Université de Savoie, CNRS/IN2P3, F-74941 Annecy-Le-Vieux, France,*
[2]*Universitat de Barcelona, Facultat de Fisica, Departament ECM, E-08028 Barcelona, Spain*
[3a]*INFN Sezione di Bari, I-70126 Bari, Italy*
[3b]*Dipartimento di Fisica, Università di Bari, I-70126 Bari, Italy*
[4]*University of Bergen, Institute of Physics, N-5007 Bergen, Norway*
[5]*Lawrence Berkeley National Laboratory and University of California, Berkeley, California 94720, USA*
[6]*Ruhr Universität Bochum, Institut für Experimentalphysik 1, D-44780 Bochum, Germany*
[7]*University of British Columbia, Vancouver, British Columbia, Canada V6T 1Z1*
[8]*Brunel University, Uxbridge, Middlesex UB8 3PH, United Kingdom*
[9]*Budker Institute of Nuclear Physics, Novosibirsk 630090, Russia*
[10]*University of California at Irvine, Irvine, California 92697, USA*
[11]*University of California at Riverside, Riverside, California 92521, USA*
[12]*University of California at Santa Barbara, Santa Barbara, California 93106, USA*
[13]*University of California at Santa Cruz, Institute for Particle Physics, Santa Cruz, California 95064, USA*
[14]*California Institute of Technology, Pasadena, California 91125, USA*
[15]*University of Cincinnati, Cincinnati, Ohio 45221, USA*
[16]*University of Colorado, Boulder, Colorado 80309, USA*
[17]*Colorado State University, Fort Collins, Colorado 80523, USA*
[18]*Technische Universität Dortmund, Fakultät Physik, D-44221 Dortmund, Germany*
[19]*Technische Universität Dresden, Institut für Kern- und Teilchenphysik, D-01062 Dresden, Germany*
[20]*Laboratoire Leprince-Ringuet, CNRS/IN2P3, Ecole Polytechnique, F-91128 Palaiseau, France*
[21]*University of Edinburgh, Edinburgh EH9 3JZ, United Kingdom*
[22a]*INFN Sezione di Ferrara, I-44100 Ferrara, Italy*
[22b]*Dipartimento di Fisica, Università di Ferrara, I-44100 Ferrara, Italy*
[23]*INFN Laboratori Nazionali di Frascati, I-00044 Frascati, Italy*
[24a]*INFN Sezione di Genova, I-16146 Genova, Italy*
[24b]*Dipartimento di Fisica, Università di Genova, I-16146 Genova, Italy*
[25]*Indian Institute of Technology Guwahati, Guwahati, Assam, 781 039, India*
[26]*Harvard University, Cambridge, Massachusetts 02138, USA*
[27]*Harvey Mudd College, Claremont, California 91711*
[28]*Universität Heidelberg, Physikalisches Institut, Philosophenweg 12, D-69120 Heidelberg, Germany*
[29]*Humboldt-Universität zu Berlin, Institut für Physik, Newtonstr. 15, D-12489 Berlin, Germany*
[30]*Imperial College London, London, SW7 2AZ, United Kingdom*
[31]*University of Iowa, Iowa City, Iowa 52242, USA*
[32]*Iowa State University, Ames, Iowa 50011-3160, USA*
[33]*Johns Hopkins University, Baltimore, Maryland 21218, USA*
[34]*Laboratoire de l'Accélérateur Linéaire, IN2P3/CNRS et Université Paris-Sud 11, Centre Scientifique d'Orsay, B. P. 34, F-91898 Orsay Cedex, France*
[35]*Lawrence Livermore National Laboratory, Livermore, California 94550, USA*
[36]*University of Liverpool, Liverpool L69 7ZE, United Kingdom*
[37]*Queen Mary, University of London, London, E1 4NS, United Kingdom*
[38]*University of London, Royal Holloway and Bedford New College, Egham, Surrey TW20 0EX, United Kingdom*
[39]*University of Louisville, Louisville, Kentucky 40292, USA*
[40]*Johannes Gutenberg-Universität Mainz, Institut für Kernphysik, D-55099 Mainz, Germany*
[41]*University of Manchester, Manchester M13 9PL, United Kingdom*

[42]*University of Maryland, College Park, Maryland 20742, USA*
[43]*University of Massachusetts, Amherst, Massachusetts 01003, USA*
[44]*Massachusetts Institute of Technology, Laboratory for Nuclear Science, Cambridge, Massachusetts 02139, USA*
[45]*McGill University, Montréal, Québec, Canada H3A 2T8*
[46a]*INFN Sezione di Milano, Università di Milano, I-20133 Milano, Italy*
[46b]*Dipartimento di Fisica, Università di Milano, I-20133 Milano, Italy*
[47]*University of Mississippi, University, Mississippi 38677, USA*
[48]*Université de Montréal, Physique des Particules, Montréal, Québec, Canada H3C 3J7*
[49a]*INFN Sezione di Napoli, I-80126 Napoli, Italy*
[49b]*Dipartimento di Scienze Fisiche, Università di Napoli Federico II, I-80126 Napoli, Italy*
[50]*NIKHEF, National Institute for Nuclear Physics and High Energy Physics, NL-1009 DB Amsterdam, The Netherlands*
[51]*University of Notre Dame, Notre Dame, Indiana 46556, USA*
[52]*Ohio State University, Columbus, Ohio 43210, USA*
[53]*University of Oregon, Eugene, Oregon 97403, USA*
[54a]*INFN Sezione di Padova, I-35131 Padova, Italy*
[54b]*Dipartimento di Fisica, Università di Padova, I-35131 Padova, Italy*
[55]*Laboratoire de Physique Nucléaire et de Hautes Energies, IN2P3/CNRS, Université Pierre et Marie Curie-Paris6, Université Denis Diderot-Paris7, F-75252 Paris, France*
[56a]*INFN Sezione di Perugia, I-06100 Perugia, Italy*
[56b]*Dipartimento di Fisica, Università di Perugia, I-06100 Perugia, Italy*
[57a]*INFN Sezione di Pisa, I-56127 Pisa, Italy*
[57b]*Dipartimento di Fisica, Università di Pisa, I-56127 Pisa, Italy*
[57c]*Scuola Normale Superiore di Pisa, I-56127 Pisa, Italy*
[58]*Princeton University, Princeton, New Jersey 08544, USA*
[59a]*INFN Sezione di Roma, I-00185 Roma, Italy*
[59b]*Dipartimento di Fisica, Università di Roma La Sapienza, I-00185 Roma, Italy*
[60]*Universität Rostock, D-18051 Rostock, Germany*
[61]*Rutherford Appleton Laboratory, Chilton, Didcot, Oxon, OX11 0QX, United Kingdom*
[62]*CEA, Irfu, SPP, Centre de Saclay, F-91191 Gif-sur-Yvette, France*
[63]*SLAC National Accelerator Laboratory, Stanford, California 94309 USA*
[64]*University of South Carolina, Columbia, South Carolina 29208, USA*
[65]*Southern Methodist University, Dallas, Texas 75275, USA*
[66]*Stanford University, Stanford, California 94305-4060, USA*
[67]*State University of New York, Albany, New York 12222, USA*
[68]*Tel Aviv University, School of Physics and Astronomy, Tel Aviv, 69978, Israel*
[69]*University of Tennessee, Knoxville, Tennessee 37996, USA*
[70]*University of Texas at Austin, Austin, Texas 78712, USA*
[71]*University of Texas at Dallas, Richardson, Texas 75083, USA*
[72a]*INFN Sezione di Torino, I-10125 Torino, Italy*
[72b]*Dipartimento di Fisica Sperimentale, Università di Torino, I-10125 Torino, Italy*
[73a]*INFN Sezione di Trieste, I-34127 Trieste, Italy*
[73b]*Dipartimento di Fisica, Università di Trieste, I-34127 Trieste, Italy*
[74]*IFIC, Universitat de Valencia-CSIC, E-46071 Valencia, Spain*
[75]*University of Victoria, Victoria, British Columbia, Canada V8W 3P6*
[76]*Department of Physics, University of Warwick, Coventry CV4 7AL, United Kingdom*
[77]*University of Wisconsin, Madison, Wisconsin 53706, USA*

(Received 20 January 2011; published 13 May 2011)

Searches for B mesons decaying to final states containing a baryon and a lepton are performed, where the baryon is either Λ_c or Λ and the lepton is a muon or an electron. These decays violate both baryon and lepton number and would be a signature of physics beyond the standard model. No significant signal is observed in any of the decay modes, and upper limits in the range $(3.2–520) \times 10^{-8}$ are set on the branching fractions at the 90% confidence level.

DOI: 10.1103/PhysRevD.83.091101 PACS numbers: 13.25.Hw, 11.30.Fs, 14.80.Sv

[†]Also with Università di Perugia, Dipartimento di Fisica, Perugia, Italy.
[‡]Also with Università di Roma La Sapienza, I-00185 Roma, Italy.
[§]Now at University of South Alabama, Mobile, AL 36688, USA.
[‖]Also with Università di Sassari, Sassari, Italy.

I. INTRODUCTION

Observations show that the Universe contains much more matter than antimatter [1,2]. This suggests that there are processes that violate *CP* symmetry and baryon-number conservation [3]. However, experimentally observed *CP* violation, combined with the baryon-number violating processes that are allowed by the standard model [4], cannot explain the observed matter-antimatter asymmetry.

Baryon-number violation is a prediction of many unification theories [5,6], but the proton decay rates predicted by many of these models have not been observed. Stringent limits have been placed on the lifetime of the proton [7]. The nonobservation of proton decay has been used to constrain baryon- and lepton-number violating decays involving higher-generation quarks and leptons [8]; in that study, the upper limit on the branching fraction for $B^0 \to \Lambda_c^+ \ell^-$ is calculated to be 4×10^{-29}, where ℓ is a lepton. No upper limits are calculated for B^- decays to $\Lambda \ell^-$ or $\bar{\Lambda} \ell^-$.

We report the results of searches for the decays $B^0 \to \Lambda_c^+ \ell^-$, $B^- \to \Lambda \ell^-$, and $B^- \to \bar{\Lambda} \ell^-$, where the lepton is a muon or an electron [9]. Neither lepton number nor baryon number are conserved in these decays. This is the first measurement of the branching fractions for these decays. An observation of any of these decay processes would be a sign of new physics.

II, THE *BABAR* DETECTOR AND DATASET

The data used in this analysis were recorded with the *BABAR* detector at the PEP-II asymmetric energy e^+e^- storage ring. The data sample consists of 429.0 fb^{-1} recorded at the $\Upsilon(4S)$ resonance [$\sqrt{s} = 10.58$ GeV/c^2, where $\sqrt{s}$ is the center-of-mass (CM) energy of the e^+e^- system]. The sample contains $(471 \pm 3) \times 10^6$ $B\bar{B}$ pairs.

The *BABAR* detector is described in detail elsewhere [10]. Charged particle momenta are measured in a tracking system consisting of a five-layer, double-sided silicon vertex tracker and a 40-layer central drift chamber, immersed in a 1.5 T axial magnetic field. Photon and electron energies are measured in a CsI(Tl) electromagnetic calorimeter. The instrumented magnetic flux return (IFR) for the solenoid, instrumented with resistive plate chambers or limited streamer tubes, provides muon identification. Charged particle identification (PID) is also provided by a detector of internally reflecting Cherenkov light (DIRC) and the energy loss dE/dx measured by the silicon vertex tracker and central drift chamber. Information from all these detectors is used in the particle identification.

Simulated Monte Carlo (MC) events are generated to study detector effects. The detector response is modeled using the GEANT4 software package [11]. Large numbers of signal events are generated for the six decay modes, assuming that the B meson decays do not produce any preferred polarization of the Λ_c^+ or Λ. This sample is referred to as the signal MC. For background studies, a large sample of $B\bar{B}$ events is produced, with the B mesons decaying according to the measured branching fractions [12]. The same procedure is used to generate background samples for e^+e^- annihilation to lighter quark-antiquark pairs (u, d, s, c). These two samples are referred to as background MC.

III. OVERVIEW OF ANALYSIS

We identify B-meson candidates using two kinematic variables: the difference between half the CM energy of the colliding beams and the measured CM energy of the B candidate, ΔE; and the energy-substituted mass $m_{\rm ES}$ of the B candidate. In the calculation of $m_{\rm ES}$, the precise knowledge of the initial state energy is used to improve the resolution on the calculated mass of the B candidate: $m_{\rm ES} = \sqrt{[(s/2 + \vec{p}_i \cdot \vec{p}_B)/E_i]^2 - |\vec{p}_B|^2}$, where $(E_i, \vec{p}_i)$ and $\vec{p}_B$ are, respectively, the four-momentum of the e^+e^- system and the three-momentum of the B-meson candidate in the laboratory frame. A region of phase space in these two variables, in which fits will be performed to extract the signal yield, is defined by the ranges $-0.2 < \Delta E < 0.2$ GeV and $5.2 < m_{\rm ES} < 5.3$ GeV/c^2. This is referred to as the fitting region. The signal for true B candidates for the studied decays is centered around $\Delta E = 0$ ($\sigma \approx 16$ MeV) and $m_{\rm ES} = 5.279$ GeV/c^2 ($\sigma \approx 3$ MeV/c^2), where σ is the experimental resolution.

In any search for a rare or new process, it is important to minimize experimenter's bias. To do this, a blind analysis is performed. The kinematic region of phase space that would be populated by true signal events is hidden during optimization of the candidate selection criteria. We exclude events within roughly $\pm 5\sigma$ of the signal peak in $m_{\rm ES}$ and $\pm 4\sigma$ in ΔE. The nonblinded region is referred to as the sideband region. We define a region within $\pm 2.5\sigma$ of the signal peak in $m_{\rm ES}$ and ΔE as the signal region.

The signal yield is extracted with an unbinned extended maximum likelihood fit. The total probability distribution function (PDF) is a sum of PDFs for signal and background. Each of these PDFs is a product of PDFs describing the dependence on $m_{\rm ES}$ and ΔE. For the $\Lambda_c^+ \ell^-$ modes, additional discriminating power is gained from a three-dimensional PDF, where the output from a neural net discriminator is used as the third variable. This discriminator is defined in the next section.

IV. CANDIDATE SELECTION AND OPTIMIZATION

Λ_c^+ candidates are reconstructed through the decay mode $\Lambda_c^+ \to pK^-\pi^+$, which has a branching fraction of $(5.0 \pm 1.3) \times 10^{-2}$ [7]. Other studies of B decays to Λ_c^+ [13] show that including additional Λ_c^+ decay modes would add little sensitivity to this analysis. Λ candidates are reconstructed through the decay $\Lambda \to p\pi^-$, which has a branching fraction of $(63.9 \pm 0.5) \times 10^{-2}$ [7]. The final

state tracks for both the Λ_c^+ and Λ decays are constrained to a common spatial vertex and their invariant mass is constrained to the Λ_c^+ or Λ mass [7]. This has the effect of improving the four-momentum resolution for true $B \to \Lambda_{(c)}\ell$ candidates.

B-meson candidates are formed by combining a Λ_c^+, Λ, or $\bar{\Lambda}$ candidate with a μ^- or e^-. The baryon and lepton candidates are constrained to originate from a common point. The final state hadron (p, K, π) and lepton (μ, e) candidates are all required to be consistent with the candidate particle hypothesis according to PID algorithms that use dE/dx, DIRC, electromagnetic calorimeter, and IFR information. The four-momenta of photons that are consistent with bremsstrahlung radiation from the electron candidate are added to that of the electron. As the Λ has $c\tau = 7.89$ cm, the purity of the Λ-candidate sample is improved by selecting candidates for which the reconstructed decay point of the Λ candidate is at least 0.2 cm from the reconstructed decay point of the B candidate in the plane perpendicular to the e^+e^- beams.

A non-negligible background for the $\Lambda\ell$ channel is due to incorrect identification of electrons and positrons in $e^+e^- \to e^+e^-\gamma$ events in which the photon converts into an additional e^+e^- pair and an electron and positron in the final state are misidentified as a π^- and proton coming from a Λ decay. This background is almost entirely eliminated by requiring that there are more than four charged tracks in the event. We apply this selection criterion to all channels.

Candidate selection optimization is performed balancing two goals: setting the lowest upper limit while remaining sensitive to a signal. We use the Punzi figure of merit (FOM) [14], $\epsilon/(a/2 + \sqrt{N_{\rm bkg}})$, where ϵ is the signal efficiency, $N_{\rm bkg}$ is the expected number of background events, and a is the number of standard deviations of significance at which the analysts would claim a discovery. For this analysis, $a = 5$ is used. The signal efficiency and the expected number of background events are obtained from the respective MC samples.

For optimization of the p, K, π candidate PID selection, we calculate the Punzi FOM by estimating ϵ and $N_{\rm bkg}$ from the baryon candidate invariant mass distribution. The background is assumed to be linear in the baryon invariant mass and a fit is made to extract the number of signal and background candidates. After the PID selection is optimized, we select candidates within ± 15 MeV$/c^2$ of the nominal Λ_c^+ mass and ± 4 MeV$/c^2$ of the nominal Λ mass [7].

The lepton candidate selection is optimized based on the number of $B \to \Lambda_{(c)}\ell$ candidates in the signal region in MC samples. These B candidates contain correctly identified leptons from the signal decay, which define ϵ in the Punzi FOM, and two types of background, which determine $N_{\rm bkg}$: correctly identified leptons from standard model processes, and incorrectly identified leptons.

A neural net is used to provide further discrimination between signal and background. We use the TMVA software package [15] and its multilayer perceptron implementation of a neural net. The neural net is trained using MC simulated samples for signal and for $e^+e^- \to q\bar{q}$ ($q = u, d, s, c$). The six discriminating variables, all defined in the CM frame of the e^+e^- beams, used in the neural net algorithm are the angle between the B meson momentum and the axis defined by the colliding e^+e^- system, the angle between the B meson candidate sphericity [16] axis and the sphericity axis defined by the charged particles in the rest of the event (ROE), the angle between the B meson candidate thrust [16] axis and the thrust axis defined by the charged particles in the ROE, the ratio of the 2nd to 0th Fox-Wolfram moment [17] calculated from the entire event using both charged and neutral particles, L moments of the ROE tracks [18], and the magnitude of the thrust of the entire event. For the $\Lambda\ell$ modes, the ratio of the Fox-Wolfram moments and the magnitude of the thrust of the entire event show a slight correlation with ΔE and $m_{\rm ES}$ in the background sample and are therefore not used.

For the $\Lambda_c^+\ell^-$ decay modes, we retain events with a value of the neural net output above a threshold such that about 90% of the signal is retained and about 50% of the background is rejected. The neural net output for the retained events is used as a third discriminating variable in the PDF used in the fit.

The $\Lambda\ell$ modes have significantly less background than the $\Lambda_c^+\ell^-$ modes. For the $\Lambda\ell$ modes, we retain events with a value of the neural net output above a threshold (optimized using the Punzi FOM) and perform a fit in ΔE and $m_{\rm ES}$ only.

After the optimized selection criteria are applied, the remaining background for the $\Lambda_c^+\ell^-$ modes is composed of roughly equal amounts of $B\bar{B}$ and $q\bar{q}$ ($q = u, d, s, c$) events, while the background for the $\Lambda\ell$ modes is almost entirely $q\bar{q}$.

V. EXTRACTION OF RESULTS

As stated earlier, the signal yield is extracted with an unbinned extended maximum likelihood fit. For all decay modes, the signal $m_{\rm ES}$ PDF is modeled as a Crystal Ball function [19], which has three free parameters. The signal ΔE PDF is the sum of two Crystal Ball functions with the same mean. For the $\Lambda_c^+\ell^-$ decay modes, the signal neural net output is modeled by a nonparametric PDF implemented in the ROOFIT [20] package that models the distribution as a superposition of Gaussian kernels [21]. The full signal PDF is a product of these PDFs. Signal MC samples for each decay mode are used to determine the parameter values for these functions, and these values are fixed in the fit to the data.

For all decay modes, the background $m_{\rm ES}$ PDF is modeled as an ARGUS function [22] and the background ΔE PDF is modeled as a linear function. The unnormalized ARGUS function is defined as $\Psi(m) = mu^p e^{cu}$, where $p = 0.5$, $u = 1 - (m/m_0)^2$, c is the curvature parameter,

and m_0 is the kinematic cutoff above which the function is defined to be 0. We determine $m_0 = 5.290\ \mathrm{GeV}/c^2$ by a fit to the background MC events and fix this value in the fit to the data. For the $\Lambda_c^+\ell^-$ decay modes, the background neural net output PDF is modeled as a Crystal Ball function.

In the fit, the number of background events is a free parameter and the number of signal events S is the product of the branching fraction $\mathcal{B}$, which is treated as a free parameter, and a conversion factor $\mathcal{F}$: $S = \mathcal{B}\mathcal{F}$, where $\mathcal{F} = \epsilon\mathcal{B}_{\Lambda_{(c)}}N_B$, $\mathcal{B}_{\Lambda_{(c)}}$ is the branching fraction for the Λ_c^+ or Λ, and N_B is the number of either neutral or charged B mesons in the dataset; $N_B = 2N_{\Upsilon(4S)}\mathcal{B}_{B\bar{B}}$, where $N_{\Upsilon(4S)}$ is the number of $\Upsilon(4S)$ in the dataset, $\mathcal{B}_{B\bar{B}}$ is the branching fraction for the $\Upsilon(4S)$ to decay to either a neutral or charged $B\bar{B}$ pair, and the factor of 2 accounts for the pair of B mesons produced in each $\Upsilon(4S)$ decay. There are no other free parameters for the signal PDF. The two-dimensional background PDF for the $\Lambda\ell$ modes has two free parameters (the ΔE slope and the m_{ES} ARGUS shape parameter); the three-dimensional background PDF for the $\Lambda_c^+\ell^-$ modes has three additional free parameters for the Crystal Ball function that models the neural net output.

In order to incorporate systematic uncertainties on $\mathcal{F}$ (discussed below) directly in the fit and propagate them to the total uncertainty on the branching fraction, a Gaussian constraint is included as a term ($\mathcal{G}$) in the ln-likelihood function ($\ln\mathcal{L}$): $\mathcal{G} = (\mathcal{F} - \mathcal{F}_{\mathrm{fit}})^2/2\delta_{\mathcal{F}}^2$, where $\mathcal{F}$ is the value we calculate for the conversion factor, $\mathcal{F}_{\mathrm{fit}}$ is a free parameter, and $\delta_{\mathcal{F}}$ is the uncertainty on the conversion factor. The Gaussian constraint is turned off in a subsequent fit to extract the statistical uncertainty only. This error is then subtracted in quadrature from the total error to determine the systematic error on the branching fraction from these sources.

In order to test the stability and sensitivity of the fitting procedure as well as to search for possible bias in the fit, simulated signal events are embedded in a sample of background events generated from the background PDFs using MC techniques. We generate many independent samples with varying ratios of the number of embedded signal events to the number of background events in order to model different branching fractions. These samples are fit and the extracted branching fractions are compared with the branching fractions used to determine the amount of embedded signal events. Biases of no more than 20% of the statistical uncertainty on the result of an individual fit are observed, depending on the decay mode and the number of signal events. In addition, for $\mathcal{B} = 0$ fits, we observe that 0.1% to 1.5% of fits (depending on decay mode) have no candidates in the signal region, and are thus unable to constrain the signal parameters. To avoid nonmathematical negative PDF values [23], we refit these cases in the data with a constraint that the PDF must be positive throughout the fitting region.

Systematic uncertainties are due to uncertainties on Λ and Λ_c^+ branching fractions, the total number of B mesons produced during the experiment's lifetime, and the tracking and PID efficiencies, which are determined from control samples in data. We use the measured branching fractions and associated uncertainties for $\Upsilon(4S) \to B^+B^-$ and $\Upsilon(4S) \to B^0\bar{B}^0$, which are $(51.6 \pm 0.6) \times 10^{-2}$ and $(48.4 \pm 0.6) \times 10^{-2}$, respectively [24]. For the $\Lambda_c^+\ell^-$ mode, the systematic uncertainty is dominated by the 26% uncertainty on the $\Lambda_c^+ \to pK^-\pi^+$ branching fraction; the other uncertainties contribute about 3%. We do not assign any systematic uncertainty due to the assumption of an unpolarized final state. Systematic uncertainties from the fixed PDF parameters are considered to be negligible. The total systematic uncertainties are estimated to be 26%

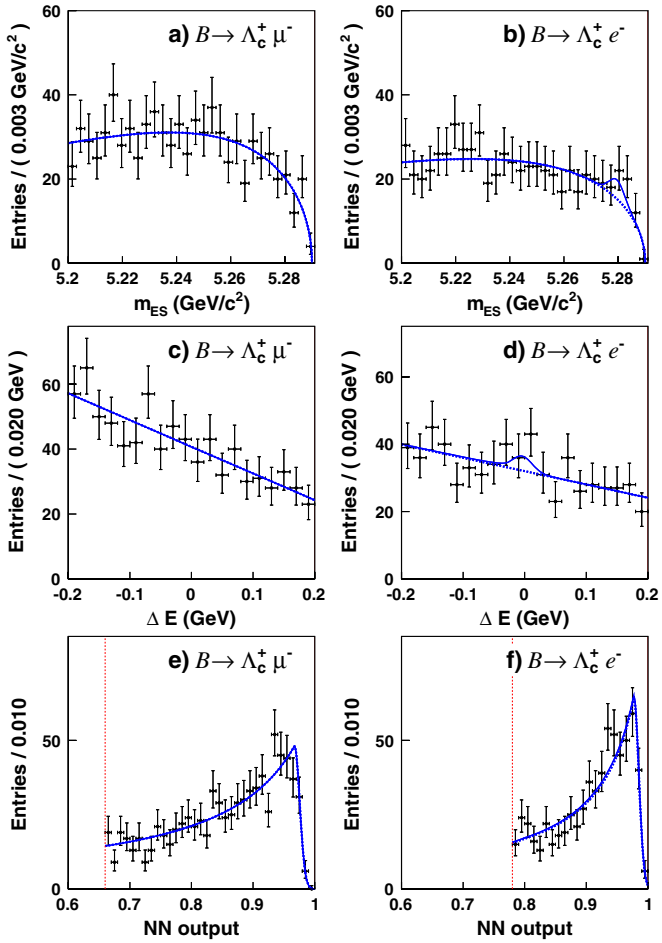

FIG. 1 (color online). Data for all events in the fitting region with overlaid fit results for $B^0 \to \Lambda_c^+\ell^-$ candidates. The left column is for the muon mode and the right column the electron mode. Distributions of (a), (b) m_{ES}; (c), (d) ΔE, and (e), (f) neural net (NN) output are shown. Dashed lines represent the background components of the fit and solid lines represent the sum of the signal and background components. The lack of a significant signal makes the solid and dashed lines indistinguishable in some plots. In panels (e) and (f), the vertical dashed line indicates the selection criteria on the neural net output.

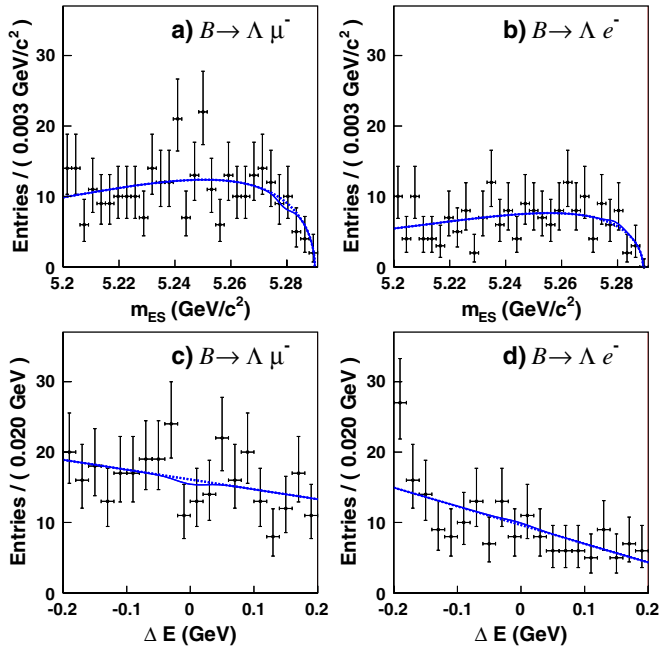

FIG. 2 (color online). Data for all events in the fitting region with overlaid fit results for $B^- \to \Lambda\ell^-$ candidates. The left column is for the muon mode and the right column the electron mode. Distributions of (a), (b) $m_{\rm ES}$ and (c), (d) ΔE are shown. Dashed lines represent the background components of the fit and solid lines represent the sum of the signal and background components. The lack of a significant signal makes the solid and dashed lines indistinguishable in some plots.

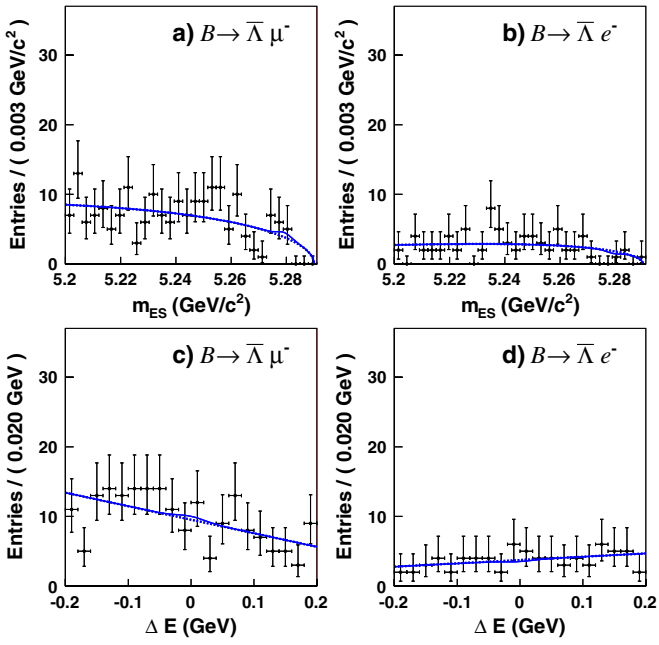

FIG. 3 (color online). Data for all events in the fitting region with overlaid fit results for $B^- \to \bar\Lambda\ell^-$ candidates. The left column is for the muon mode and the right column the electron mode. Distributions of (a), (b) $m_{\rm ES}$ and (c), (d) ΔE are shown. Dashed lines represent the background components of the fit and solid lines represent the sum of the signal and background components. The lack of a significant signal makes the solid and dashed lines indistinguishable in some plots.

for $B^0 \to \Lambda_c^+\ell^-$, 3.0% for $B^- \to \Lambda\mu^-$ and $B^- \to \bar\Lambda\mu^-$, and 2.5% for $B^- \to \Lambda e^-$ and $B^- \to \bar\Lambda e^-$.

The data and the fit projections are shown in Figs. 1–3 for $B^0 \to \Lambda_c^+\ell^-$, $B^- \to \Lambda\ell^-$, and $B^- \to \bar\Lambda\ell^-$, respectively.

VI. RESULTS

No significant signal is observed and an upper limit is calculated for the branching fraction for each decay mode. To calculate the upper limit, the branching fraction is varied around the best fit value $\mathcal{B}_{\rm best}$ and the other parameters are refit to map out the difference in the ln likelihood: $\Delta\ln\mathcal{L} = \ln\mathcal{L}(\mathcal{B}_{\rm best}) - \ln\mathcal{L}(\mathcal{B})$. We integrate the function $y = e^{-\Delta\ln\mathcal{L}}$ over $\mathcal{B}$. While the fit allows the branching fraction to assume negative values, we ignore the unphysical region with $\mathcal{B} < 0$ and calculate the integral for $\mathcal{B} > 0$. We determine the value of the branching fraction $\mathcal{B}_{90\%}$ for which 90% of the area lies between $\mathcal{B} = 0$ and $\mathcal{B}_{90\%}$ and interpret this as the upper limit at 90% confidence level. The results from the fit are given in Table I. Since the biases observed in Monte Carlo studies are small compared to the statistical uncertainties, we do not include their effect in the results. For the $\bar\Lambda e^-$ decay mode, there are no candidates in the signal region. The fitted branching fraction for this decay mode is equal to the limit in the fit determined by the requirement that the PDF be positive throughout the fitting region.

TABLE I. The total number of candidates used in the fit ($N_{\rm cand}$), the central value for the branching fraction returned by the fit ($\mathcal{B}$), signal efficiency (ϵ) excluding the contribution from the $\Lambda_{(c)}$ branching fraction, and upper limits on the branching fraction at 90% confidence level ($\mathcal{B}_{90\%}$) for each decay mode are shown.

Decay mode	$N_{\rm cand}$	$\mathcal{B}$ ($\times 10^{-8}$)	ϵ (%)	$\mathcal{B}_{90\%}$ ($\times 10^{-8}$)
$B^0 \to \Lambda_c^+\mu^-$	814	-4^{+71}_{-56}	26.3 ± 0.9	180
$B^0 \to \Lambda_c^+ e^-$	651	190^{+130}_{-90}	25.7 ± 0.7	520
$B^- \to \Lambda\mu^-$	320	$-2.3^{+3.5}_{-2.5}$	28.7 ± 0.9	6.2
$B^- \to \Lambda e^-$	194	$1.2^{+3.7}_{-2.6}$	27.2 ± 0.6	8.1
$B^- \to \bar\Lambda\mu^-$	192	$1.5^{+2.6}_{-1.7}$	31.3 ± 1.0	6.1
$B^- \to \bar\Lambda e^-$	74	$-0.9^{+0.7}_{-0.0}$	30.0 ± 0.6	3.2

VII. SUMMARY

Searches are performed for the decays $B^0 \to \Lambda_c^+ \ell^-$, $B^- \to \Lambda \ell^-$, and $B^- \to \bar{\Lambda} \ell^-$, using the full *BABAR* data set. No significant signal for any of the decay modes is observed and upper limits are determined at the 90% confidence level.

ACKNOWLEDGMENTS

We are grateful for the excellent luminosity and machine conditions provided by our PEP-II colleagues, and for the substantial dedicated effort from the computing organizations that support *BABAR*. The collaborating institutions wish to thank SLAC for its support and kind hospitality. This work is supported by DOE and NSF (U.S.), NSERC (Canada), CEA and CNRS-IN2P3 (France), BMBF and DFG (Germany), INFN (Italy), FOM (The Netherlands), NFR (Norway), MES (Russia), MICIIN (Spain), STFC (United Kingdom). Individuals have received support from the Marie Curie EIF (European Union), the A. P. Sloan Foundation (U.S.), and the Binational Science Foundation (U.S.-Israel).

[1] P. Coppi, in the *Proceedings of 32nd SLAC Summer Institute on Particle Physics (SSI 2004): Nature's Greatest Puzzles* (Menlo Park, California, 2004), http://inspirebeta.net/record/671069.
[2] G. Steigman, Annu. Rev. Astron. Astrophys. **14**, 339 (1976).
[3] A. D. Sakharov, Pis'ma Zh. Eksp. Teor. Fiz. **5**, 32 (1967).
[4] V. A. Kuzmin, V. A. Rubakov, and M. E. Shaposhnikov, Phys. Lett. **155B**, 36 (1985).
[5] H. Georgi and S. L. Glashow, Phys. Rev. Lett. **32**, 438 (1974).
[6] H. Fritzsch and P. Minkowski, Ann. Phys. (N.Y.) **93**, 193 (1975).
[7] K. Nakamura (Particle Data Group), J. Phys. G **37**, 075021 (2010).
[8] W. S. Hou, M. Nagashima, and A. Soddu, Phys. Rev. D **72**, 095001 (2005).
[9] Throughout this paper, whenever a decay mode is given, the charge conjugate is also implied.
[10] B. Aubert *et al.* (*BABAR* Collaboration), Nucl. Instrum. Methods Phys. Res., Sect. A **479**, 1 (2002).
[11] S. Agostinelli *et al.* (GEANT4 Collaboration), Nucl. Instrum. Methods Phys. Res., Sect. A **506**, 250 (2003).
[12] D. J. Lange, Nucl. Instrum. Methods Phys. Res., Sect. A **462**, 152 (2001).
[13] B. Aubert *et al.* (*BABAR* Collaboration), Phys. Rev. D **78**, 112003 (2008).
[14] G. Punzi, in the *Proceedings of PHYSTAT2003: Statistical Problems in Particle Physics, Astrophysics, and Cosmology* (Menlo Park, California, 2003), p. 79, http://inspirebeta.net/record/634798.
[15] A. Hoecker *et al.*, Proc. Sci., ACAT2007 (2007) 040.
[16] A. De Rujula, J. R. Ellis, E. G. Floratos, and M. K. Gaillard, Nucl. Phys. **B138**, 387 (1978).
[17] G. C. Fox and S. Wolfram, Nucl. Phys. **B149**, 413 (1979).
[18] L moments are defined as $L_i \equiv \sum_j p_j^* \cdot |\cos\theta_j^*|^i / \sum_j p_j^*$ where p_j^* and θ_j^* are the momentum and angle with respect to a given axis, respectively, for each particle j.
[19] M. J. Oreglia, Ph.D. thesis [Report No. SLAC-R-236, 1980], Appendix D; J. E. Gaiser, Ph.D. thesis [Report No. SLAC-R-255, 1982], Appendix F; T. Skwarnicki, Ph.D. thesis [Report No. DESY-F31-86-02, 1986], Appendix E.
[20] W. Verkerke and D. P. Kirkby, in the *Proceedings of 2003 Conference for Computing in High-Energy and Nuclear Physics (CHEP 03)* (La Jolla, California2003), p. 186, http://inspirebeta.net/record/62139.
[21] K. S. Cranmer, Comput. Phys. Commun. **136**, 198 (2001).
[22] H. Albrecht *et al.* (ARGUS Collaboration), Phys. Lett. B **185**, 218 (1987).
[23] F. C. Porter (*BABAR* Collaboration), Report No. CALT 68-2463, SLAC-PUB-10243.
[24] B. Aubert *et al.* (*BABAR* Collaboration), Phys. Rev. Lett. **95**, 042001 (2005).